energies

MDPI

Article

Optimizing High-Voltage Direct Current Transmission Corridors: Dynamic Thermal Line Rating for Enhanced Renewable Generation and Greenhouse Gas Emission Reductions

Veenavi Pemachandra, Petr Musilek * and Gregory Kish

Electrical and Computer Engineering, University of Alberta, Edmonton, AB T6G 1H9, Canada; pemachan@ualberta.ca (V.P.); gkish@ualberta.ca (G.K.)
* Correspondence: pmusilek@ualberta.ca

Abstract: Recently, significant attention has been paid to the large-scale use of renewable energy through high-voltage direct current (HVDC) because of its economic feasibility. At the same time, the growing demand for electricity and the increasing penetration of renewable energy sources have prompted the electric power industry to explore methods to optimize the use of the existing grid infrastructure. Dynamic thermal line rating (DTLR) is a technique that allows transmission lines to operate at their maximum capacity, considering their real-time operating conditions. The majority of existing research on this topic has focused predominantly on employing DTLR in alternating current systems and exploring their applications. This study presents a novel approach by applying DTLR to HVDC transmission corridors, with the aim of maximizing the utilization of their capacity and facilitating increased integration of renewable energy. The performance of the proposed approach is evaluated by conducting a case study for an HVDC transmission line in Alberta, Canada. On average, the mean increase in ampacity above the static rating is 64% during winter and 34% during summer. This additional capacity can be used to integrate wind energy, replacing coal-fired generation. This leads to a significant reduction in greenhouse gas emissions, also quantified in this contribution.

Keywords: dynamic line rating; HVDC transmission; conductor temperature; greenhouse gas emission; renewable energy sources

check for updates

Citation: Pemachandra, V.; Musilek, P.; Kish, G. Optimizing High-Voltage Direct Current Transmission Corridors: Dynamic Thermal Line Rating for Enhanced Renewable Generation and Greenhouse Gas Emission Reductions. *Energies* **2024**, *17*, 2318. https://doi.org/10.3390/en17102318

Academic Editor: Zheng Xu

Received: 20 December 2023
Revised: 7 May 2024
Accepted: 8 May 2024
Published: 11 May 2024

Copyright: © 2024 by the authors. Licensee MDPI, Basel, Switzerland. This article is an open access article distributed under the terms and conditions of the Creative Commons Attribution (CC BY) license (https://creativecommons.org/licenses/by/4.0/).

1. Introduction

Recent economic growth has resulted in a significant increase in electrical consumption, driving an increase in the demand for electrical power [1,2]. This will require the addition of more capacity in all parts of the electrical system, including generation, transmission, and distribution. However, the addition of new infrastructure not only increases costs, but also construction time [3]. As a result, power utilities, government organizations, and professional bodies are exploring ways to optimally utilize the existing power system infrastructure [4]. The main component that limits power transfer is not only the generation plant itself, but also the transmission lines that carry power from the plants to the substations [3]. The ampacity of the conductors in transmission and distribution lines depends on the maximum allowable conductor temperature. Factors such as sag and tension often limit this temperature. The rating considered by the utilities, which is known as the "nominal rating" or "static rating (SR)", is calculated by considering worst-case weather conditions, which are often very conservative. The weather parameters typically used to calculate the SR are a wind speed of 0.6 ms^{-1}, a 40 °C ambient temperature, and a solar radiation of 1000 Wm^{-2} [5]. It should also be noted that the simultaneous occurrence of these conditions is unlikely in real-world scenarios [2]. Consequently, the SR of overhead lines is usually much lower than the actual ampacity of the line. The dynamic thermal line rating (DTLR) represents the actual current that the conductor could carry at a given time by incorporating real-time weather conditions. It allows transmission system operators to

move more power from existing transmission corridors while maintaining a safe operating environment. Due to its many advantages, DTLR has recently been employed in many transmission and distribution applications and has also been an important topic of research.

Research on overhead conductors, which also leads to the topic of DTLR, goes back to the period before World War 2 [6]. Around this time, several studies were developed regarding the heat transfer of conductors in still air, but a major experiment was based on the forced convection of conductors, conducted in 1930 by Schurig and Frick [7]. The results were used until recently; however, the actual behavior of wind speed, direction, and gustiness made it challenging to accept their observed results. In 1959, House and Tuttle investigated the current temperature characteristics of ACSR conductors [8], where a current-carrying capacity formula was derived considering the conductor's heat loss and heat gain due to the effects of wind, solar radiation, ambient temperature, and surface conditions. However, the first academic article that applied the thermal rating of overhead conductors using real-time weather conditions [9] was published in 1977.

Since then, this topic has been widely studied and researched in various geographical regions, mainly for alternating current (AC) systems and their applications, with proven results. In 2000, Raniga and Rayudu [10] described a real-time application of the New Zealand transmission system using the line tension monitoring method. In 2008, the DTLR was calculated based on meteorological data for a 132 kV double circuit transmission line in England. It was found that 20% to 50% more wind energy can be incorporated [11]. In 2011, a pilot experiment on a sag monitoring device known as 'Ampacimon' was conducted for a 400 kV twin conductor line in France. The real-time line ampacity was calculated, incorporating the measured sag measurements and most of the time resulting in the line having more capacity than the static rating by at least 20% [12]. In 2013, a case study was conducted for a double-circuit transmission line in Korea to analyze the benefits of using DTLR. The results showed that the maximum allowable load can be increased by up to 135% [13]. In 2015, the Idaho National Laboratory in collaboration with Alberta TSO, Altalink, conducted a study on a weather-based DLR system called GLASS, concluding that there is a minimum of a 22% increase in ampacity 76% of the time [4]. In 2023, Glaum and Hofmann [14] discussed a German case study on the potential of optimizing and using the grid capacity more efficiently. This was not just limited to overhead transmission systems; the researchers also extended this concept to applications for distribution systems [15] as well as underground systems [16]. Nevertheless, considering the previous research, the majority has focused predominantly on employing DTLR in AC systems and its presence in DC applications is limited. Borbáth et al. [17] discuss how the dynamic capacity of HVDC interconnectors can allow HVDC system operators to increase their profits and provide faster investment recovery. However, a thorough investigation of the theoretical understanding of how a dynamic rating is achieved in HVDC interconnectors has yet to be conducted.

With the growing awareness of climate change and its negative impacts, many sectors that generate greenhouse gases (GHGs) are concentrating on reducing their emissions [18]. Canada, along with many other countries, pledged to achieve net zero emissions by 2050 during the United Nations Climate Change Conference in Glasgow in 2021 (COP26). Therefore, the electricity sector, one of the major contributors to GHG emissions, is under pressure to adopt zero-emission power generation technologies [19] such as renewable energy projects [20] and green generation options including wind, solar, geothermal, biomass, and small hydro to reduce reliance on fossil fuels [21].

With this recent movement of utilities towards renewable energy sources, significant attention has been paid to the incorporation of wind energy into the power system using DTLR, which uses cold weather and wind to cool down the overheated transmission lines, increasing their thermal capacity [22]. A field study was conducted in N. Ireland to develop a statistical model to calculate the DTLR for a wind-intensive area [23] using line current and weather data. Schell et al. [24] presented a situation in Belgium, in which the Belgian TSO was required to add more wind power to their 70 kV network, which was already saturated

with the traditional calculations. Talpur et al. [25] investigate dynamic rating calculations for a 130 kV sub-transmission system to check the feasibility and best location to integrate a 60 MW wind power park in the same line. In conclusion, the relationship between wind energy and dynamic ratings holds the possibility of integrating more renewable energy while reducing network congestion.

With the expansion of electricity demand and the growth in renewable generation, the grid is becoming more decentralized, with some generation sources located at greater distances from consumers [26]. As a result, utilities are exploring more economical long-distance transmission options, such as HVDC, which has brought the overloading capability of transmission lines in general and in HVDC systems in particular to our attention. The overload capability of HVDC can be categorized into three categories depending on the duration of overload: continuous, short-time, and transient. Known systems have a broad range of short-term overload capabilities, spanning from 1 to 8 h, and a transient overload range of 3 to 15 s. Line commutated converters (LCCs), which consist of thyristor valves, and voltage source converters (VSCs), which utilize insulated-gate bipolar transistor (IGBT) switches, have distinct overloading capacities. Notably, LCC-based HVDC systems have a higher capacity to withstand overload compared to VSC-based systems [27]. The 50 MW overload capacity of the BritNed LCC-HVDC link [28], 20 MW overload capacity of Nemolink VSC-HVDC [29], 15 MW overload capacity of Eastlink-1 VSC-HVDC and 16 MW overload capacity of Eastlink-2 LCC-HVDC [30] are some of the known examples of using the overload capacity of HVDC systems in real-time applications. However, when DTLR is implemented in HVDC systems, the overload capabilities of their components must also be considered. This rating depends on the thermal rating of key components of the system, such as the converter transformer, power electronic devices, and conductors, as well as the cooling systems and the ambient temperature [31]. Extensive care must be taken if the converters are overloaded while the conductor operates at its dynamic rating.

Considering the current situation of renewables in the province of Alberta (southern Alberta is identified as more favorable for wind and solar), there is a need to transfer power over long distances from the south to the north. As Calgary, Red Deer, and Edmonton are the three largest cities in Alberta, responsible for one-third of the provincial load, transmission system operators plan to use the two HVDC lines, which are the Eastern Alberta Transmission Line (EATL) and the Western Alberta Transmission Line (WATL), as the transmission corridor between north and south [32]. Further, the Alberta Electric System Operator (AESO) [33] reports a maximum capacity of 3853 MW for wind and 1292 MW for solar. It is also evident that these numbers will increase significantly by 2035, as forecasted for different scenarios [19]. According to the AESO, many renewable energy projects were added in 2021 and 2022, including 718 MW of solar projects and 1547 MW of wind power projects [19]. After implementing these projects, there are further plans for additional solar and wind to come from corporate power purchase agreements (PPAs) and distributed energy resources (DERs). This raises concerns about whether the existing system is adequate to integrate additional clean energy generation without significant investment in infrastructure development.

In conclusion, the increase in electricity demand has resulted in an improvement in the existing transmission infrastructure as well as the need for long-distance transmission such as HVDC systems. The overview of DTLR, coupled with the examples of past studies, establishes a better understanding of the evolution of the technique and how it has been used in real-time networks. However, a notable gap in the literature surfaces—the existing studies on DTLR predominantly experiment with AC systems. This study steps into the spotlight by bringing in a novel approach: adding DTLR to HVDC transmission corridors, intending to maximize the utilization of their capacity and facilitate an increased integration of renewable energy. The primary objective of this study is to maximize the capacity utilization of HVDC transmission corridors and facilitate the increased integration of renewable energy by utilizing DTLR. The excess capacity gained by DTLR is used to integrate renewable energy into the grid to meet demand. In this way, GHG emissions can

be reduced by replacing the energy supplied by conventional power plants with renewable sources, and this reduction can be quantified. This study contributes to the reduction in GHG emissions by facilitating the integration of more renewable energy into the generation mix, thereby advancing the goal of achieving net-zero emissions. Furthermore, this study encouraged the adoption of DTLR in future HVDC systems in practical aspects as well as from a research perspective.

2. Principles of the Dynamic Thermal Line Rating (DTLR)

2.1. Overview of Technical Standards

The two most commonly used technical standards for calculating the DTLR are CIGRE WG B2.43 [34] and IEEE Std. 738-2012 [35]. To calculate the heat gain and loss of the conductor, both standards consider meteorological parameters such as the wind speed and direction, ambient temperature, and heat from solar radiation. Furthermore, conductor physical properties are also taken into account, i.e., the conductor diameter, conductor material properties (such as electrical conductivity), and conductor surface conditions (primarily emissivity and absorptivity).

Both the IEEE Std. 738 and CIGRE standards emphasize that 60 Hz conductor resistances given by the conductor manufacturers already incorporate considerations for skin effect and current magnitude [35]. Compared to the IEEE method, the CIGRE method introduces three additional components: evaporative cooling, magnetic heating, and corona heating. However, both standards generally dismiss evaporative and corona heating due to their probabilistic nature and accounting for magnetic heating through AC resistance [36,37]. The main differences between the two standards include the method of calculating solar heating and the convective cooling algorithm [38]. The slight differences in these calculations usually vary by 5–15% in value between these two standards, but both procedures depend on solving the heat balance equation of the conductor [36].

This concept is predominantly applied in AC systems, and there is only a limited presence in DC applications. Interestingly, the CIGRE standard explicitly highlights the applicability of thermal rating calculations for both AC and DC operation, particularly in high-temperature and high-current-density scenarios. This opens up the possibility of extending the use of this concept to HVDC systems. In this study, the IEEE Std 738 is used to calculate the steady-state thermal rating of the line, as it offers a more straightforward yet effective solution that aligns with the requirements.

2.2. Mathematical Formulation

Figure 1 depicts the state under heat balance of an overhead conductor. Under steady-state conditions, where the line loading characteristics remain consistent over an extended period of time, the heat balance equation for a single conductor is given by Equation (1) [35].

$$\text{Heat Loss} = \text{Heat Gain}$$

$$q_c + q_r = q_j + q_s \tag{1}$$

where

q_c convective cooling [W/m].
q_r radiative cooling [W/m].
q_j joule heating [W/m].
q_s solar heating [W/m].

Joule heating (q_j) is caused by the flow of current (I) through the conductor converting the electrical energy into heat due to its inherent resistance $R_{T_{avg}}$ [35]:

$$q_j = I^2 \times R_{T_{avg}} \tag{2}$$

The solar heat input to the conductor q_s is determined as follows

$$q_s = \alpha \times Q_{se} \times \sin(\theta) \times A', \tag{3}$$

where A' is the projected conductor area, Q_{se} is the overall heat intensity radiated from the sun and sky adjusted for elevation, α is the solar absorptivity, and θ is the conductor latitude.

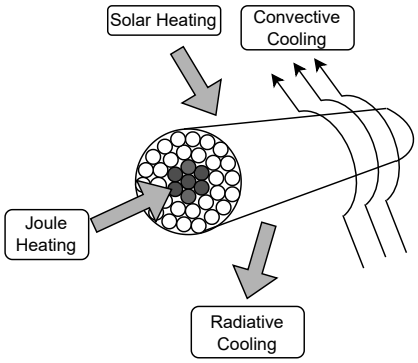

Figure 1. Heat balance of an overhead conductor.

Convective heat loss q_c is a combination of natural convection (q_{cn}) in Equation (4) and forced convection. IEEE Std. 738 [35] adopts the higher value between natural and forced convection. Natural convection is a function of the air temperature, (T_s), conductor temperature (T_a), air density (ρ_f) and conductor diameter (D_o).

$$q_{cn} = 3.645 \times \rho_f^{0.5} \times {D_o}^{0.75} \times (T_s - T_a)^{1.25}. \tag{4}$$

Forced convection is further classified into two equations: one for low wind speeds

$$q_{c1} = K_{\text{angle}} \times [1.01 + 1.35 \times N_{re}^{0.52}] \times K_f \times (T_s - T_a), \tag{5}$$

and the other for high wind speeds

$$q_{c2} = K_{\text{angle}} \times 0.754 \times N_{re}^{0.6} \times K_f \times (T_s - T_a). \tag{6}$$

Both Equations (5) and (6) depend on the wind velocity (V_W), dynamic viscosity of the air (μ_f), the coefficient of thermal conductivity of the air (K_f) and the air density (ρ_f). To find q_{c1} and q_{c2}, the wind direction factor (K_{angle}) and Reynolds number (N_{re}) must also be calculated as follows

$$K_{\text{angle}} = 1.194 - \cos(\phi) + 0.194\cos(2\phi) + 0.368\sin(2\phi) \tag{7}$$

$$N_{re} = \frac{D_o \times \rho_f \times V_W}{\mu_f} \tag{8}$$

where ϕ is the angle between the wind direction and the conductor axis.

The radiated heat loss

$$q_r = 17.8 \times D_o \times \epsilon \times \left[\left(\frac{T_s + 273}{100} \right)^4 - \left(\frac{T_a + 273}{100} \right)^4 \right] \tag{9}$$

signifies the energy emitted to the surroundings through radiation when the conductor's temperature exceeds that of its environment.

Once the parameters are determined for the fundamental principle (1), the maximum allowable current of the overhead line can be calculated as:

$$I_{rms} = \sqrt{\frac{q_c + q_r - q_s}{R_{T_{avg}}}} \tag{10}$$

When calculating the line rating for a long transmission line, the process starts by identifying the maximum allowable temperature of the conductor. Subsequently, the line is divided into sections as in Figure 2, either by equal distance or at locations where weather parameters are available. Following this division, the rating for each section is calculated. Finally, the ampacity for the entire line is calculated with the minimum value taken from all the sections for the particular period under consideration:

$$A(t) = \min_i A_i(t) \tag{11}$$

where A_i is the conductor current rating at a given point i during time t [18]. Thereby, the amount of actual power that can be transmitted by a DC transmission line can be quantified.

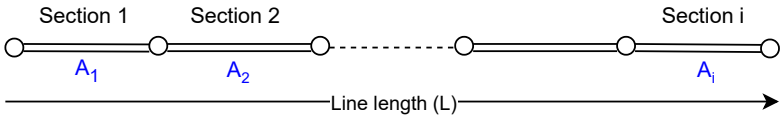

Figure 2. Transmission line divided into sections.

2.3. Methods for Determining Dynamic Thermal Line Ratings

Determining the DTLR relies on monitoring and measuring the conditions of the conductor such as the ambient, thermal, or mechanical [39] conditions. Different types of measuring technologies are available today in the market which can then be used to determine the thermal rating of a conductor.

1. Thermal state monitoring:
   The thermal-monitoring-based approach relies on measuring the conductor temperature in real time to understand the line loading [39,40]. These devices are usually driven by the magnetic field generated by the conductor current. The Power Donut Line Monitor [41,42], smART SMT Sensor [40], FMC-T6, OTLM Device, Lindsey TLM system, and EMO are some examples. These devices are capable of measuring either all or a few of the following: the root mean square (RMS) current, voltage, power, conductor temperature, surface temperature, vibration, and sag [43].
2. Mechanical state monitoring:
   Mechanical-based approaches are based on measuring the line tension, sag, or clearance to the ground. The measured quantities can then be used to calculate the line temperature which is directly proportional to sag and inversely proportional to tension and clearance [39]. CAT-1 is a commercially available tension monitoring device that also has a separate system to measure the weather parameters indirectly [44]. The Sagometer, which is based on image processing, is the only commercially available technology for real-time sag monitoring. There are some other proposed systems such as Ampacimon which measures sag via vibrations [40].
3. Weather parameter monitoring:
   Monitoring weather parameters such as the ambient temperature, wind speed, wind direction, and solar radiation is an indirect method of calculating the DTLR. This is the simplest yet the least disturbing system, as it is not necessary to install sensors on the line nor does it require any sort of communication methods such as fiber optic or satellite. Instead, the weather stations installed at the substations can be used [39].

The majority of these techniques include direct methods requiring the installation of sensors, sensor networks, and communication devices on the line.

3. GHG Emissions from the Electric Sector

A growth in electricity demand results in an increase in the amount of power generated from fossil fuels, which contributes to the increase in GHG emissions and climate change. As a consequence, electric power generation utilities are paying significant attention to reducing emissions from existing power plants and increasing renewable energy generation [45]. Table 1 provides a comprehensive overview of GHG emissions over the life cycle of each type of generation technology. According to this table, coal-fired power plants are the second greatest contributor to CO_2 emissions. In contrast, wind power stands as one of the most eco-friendly generation technologies, emitting only 3–22 g of CO_2 per kWh.

Table 1. Average GHG emissions over life cycle by each generation technology [18].

Technology	Avg. CO_2 per kWh
Wood	1500 g
Coal	800–1050 g
Natural gas	430 g
Photovoltaic solar	60–150 g
Nuclear	6 g
Hydro	4 g
Wind	3–22 g

Table 2 lists the key pollutants generated by coal-fired plants, which are not only CO_2, but also other toxic materials such as mercury [18]. This emphasizes the urgency of switching to green energy sources and also the importance of research in addressing the challenges caused by conventional electricity production methodologies.

Table 2. Key pollutants discharged by coal power plants [18].

Compound	Avg. CO_2 per kWh
Carbon Dioxide (CO_2)	371.95 g
Sulphur Dioxide (SO_x)	2.72 g
Nitrogen Oxides (NO_x)	1.81 g
Methane (CH_4)	476.27 g
Mercury (H_g)	4.08×10^{-7} g

In the context of this research, these values are used to assess emission reductions by applying DTLR strategies to incorporate more renewable energy. This evaluation confirms the environmental impact of adding more renewables such as wind energy to the mix. The use of DTLR is an important enabling factor to minimize GHG emissions.

4. HVDC System Case Study for DTLR Analysis

4.1. Study System

The potential study system configuration is illustrated in Figure 3. This system represents the Eastern Alberta Transmission Line (EATL) which spans 485 km and operates as a $\pm$500 kV HVDC link. Figure 4 illustrates the EATL and the Jenner wind farm which is conveniently located close to each other. The line was constructed between the Gibbons area, northeast of Edmonton, and the Brooks area Southeast of Calgary, as shown in Figure 5. Currently, the line is operated as a 1000 MW monopolar system, but conductors for a second pole have been installed in this line so that it can be converted to a bipolar operation. This upgrade will effectively double the transfer capability when needed in the future [32]. The conductors that carry the power from the EATL are 1590 ACSR Falcon wires with the specifications provided in Table 3.

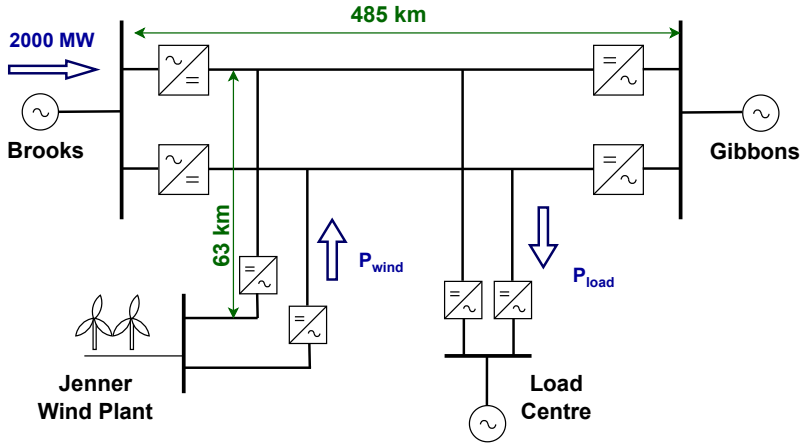

Figure 3. Study system configuration.

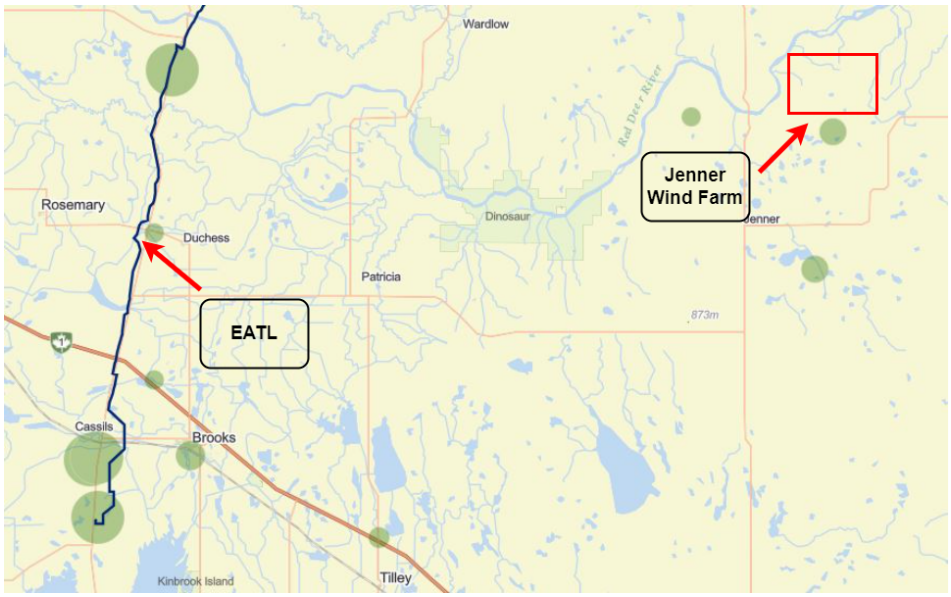

Figure 4. Location map of the EATL and Jenner wind farm.

Table 3. Assumed HVDC line conductor parameters.

Parameter	Value
Conductor type	1590 Falcon
Nominal rating	1359 A
Inside diameter	13.08 mm
Outside diameter	39.22 mm
DC resistance at 20 °C	0.035433 Ω/km
DC resistance at 50 °C	0.0401 Ω/km
Absorptivity	0.8
Emissivity	0.8

Renewable integration is carried out by incorporating the Jenner wind farm (JWPP2) [46], as shown in Figure 3. The Jenner Wind Power Project (JWPP) is one of the many renewable energy projects planned to be added to Alberta's electric system. It is located near the town of Jenner in southeast Alberta. The total project consists of three phases [46]: JWPP, JWPP2 and JWPP3. Among these, JWPP and JWPP3 are already in operation. JWPP2 will consist of 13 Enercon E160 turbines, each with a nameplate capacity of 5.49 MW, for a total capacity of 71.4 MW.

In the context of this study, several assumptions were deliberately used to simplify this case. It was taken into account that the EATL is a ±500 kV HVDC bipolar link that can transfer a maximum of 2000 MW power (1000 MW per pole). The power produced from JWPP2 is fed into the EATL, even though it might be connected to the AC transmission in the actual scenario. The wind farm specifications considered for this study are provided in Table 4, while the turbine power curve is shown in Figure 6 [47]. Further assumptions include that the power generated from the wind farm is delivered to the EATL and harnessed at an intermediate point of the line. Additionally, it is assumed that the tap to the load center functions solely as an inverter in this study.

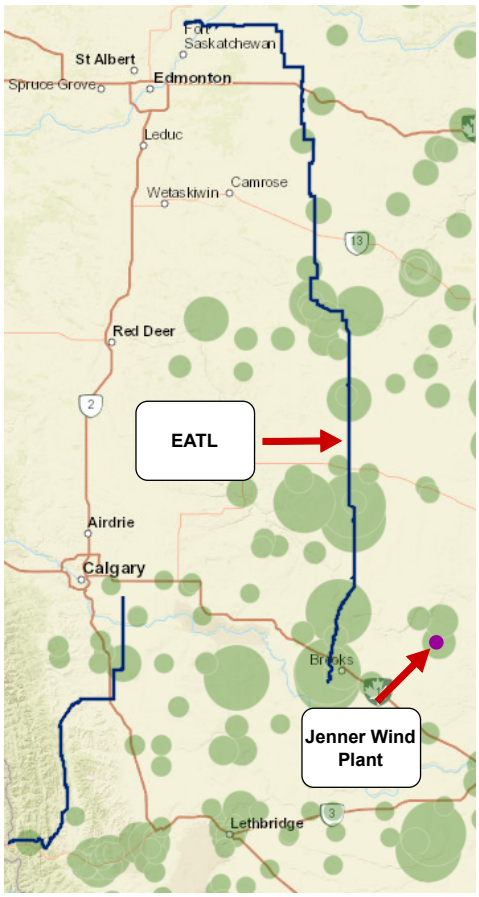

Figure 5. Span of the EATL in the province of Alberta, Canada.

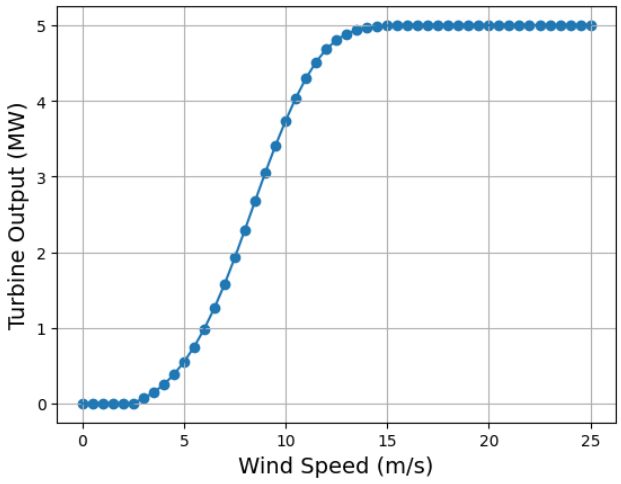

Figure 6. Power curve for an Enercon E-147 5MW turbine [47].

Table 4. Jenner wind farm specifications.

Parameter	Value
Turbine model	Enercon E-147
Number of turbines	13
Rated Power	5000 kW
Cut-in speed	2.5 m/s
Cut-out speed	25 m/s
Hub height	126 m

4.2. Meteorological Data Collection

In this study, the acquisition of accurate historical weather data is important to calculate the DTLR. Initially, consideration was given to all weather stations close to the EATL, identifying a total of 23 weather stations along and close to the line. In addition, the selection was narrowed down by choosing stations that provided all the necessary weather parameters essential for the investigation.

Consequently, six weather stations were chosen—Andrew AGDM, Brooks, Fleet AGCM, Killam AGDM, Pollockville AGDM and Vegreville—where comprehensive meteorological data on ambient temperature in °C, wind speed (km/h), wind direction (°), and solar radiation (W/m^2) were available. These data were acquired from the Current and Historical Alberta Weather Station Data Viewer online web resource provided by the Agriculture and Irrigation, Alberta Climate Information Service (ACIS) [48].

For the assessment of the wind energy production of the plant, the same ACIS platform was utilized [48]. Hourly wind data from the Atlee AGCM weather station, situated close to the JWPP2 wind farm location, were obtained to ensure accurate calculations.

4.3. Calculation Methodology

By adopting the weather station selection approach, the HVDC transmission line was divided into five distinct sections, as in Figure 2. Hourly weather data for both summer and winter seasons were procured for each designated weather station. The summer period spans from 1 May to 31 October, while the winter period covers from 1 November to 30 April each year. Subsequently, the line ampacity was determined by solving the heat balance Equation (1) for the maximum conductor temperature of 70 °C.

In this study, we performed two key calculations to assess the impact of DTLR on the EATL. Initially, the DTLR technique was applied by incorporating the acquired weather data and heat balance Equation (1). This allowed for the determination of the total power the HVDC line can transmit with DTLR, along with the additional power achievable beyond the nominal line rating. The subsequent estimation considered that the additional power is solely produced by renewable energy sources connected to the line, estimating possible reductions in GHG emissions through the replacement of coal-fired power facilities with renewable energy.

The second calculation explored the integration of the JWPP2 plant with the HVDC line, as depicted in Figure 3. The amount of energy that could be generated by the plant was calculated considering the wind data available from the nearest weather station to the plant (the Atlee AGCM). Leveraging the previously calculated DTLR, the optimal number of wind turbines needed to fully utilize the transmission line without need for additional infrastructure development was then determined.

5. Results

5.1. Dynamic Thermal Line Rating Calculation

The DTLR was calculated for a single Falcon wire conductor following the methodology described in Section 2.2. The results are visualized in Figure 7, showing the calculated DTLR values for the six winter months from 1 November 2021 to 31 April 2022, alongside the distribution histograms illustrating the percentage current gain in Figure 8. The purple dotted line represents the SR for reference. Similarly, Figure 9 shows the calculated hourly DTLR values for the summer period spanning from 1 May 2022 to 31 October 2022, while Figure 10 provides a visual representation of the percentage gain in currents during the summer months.

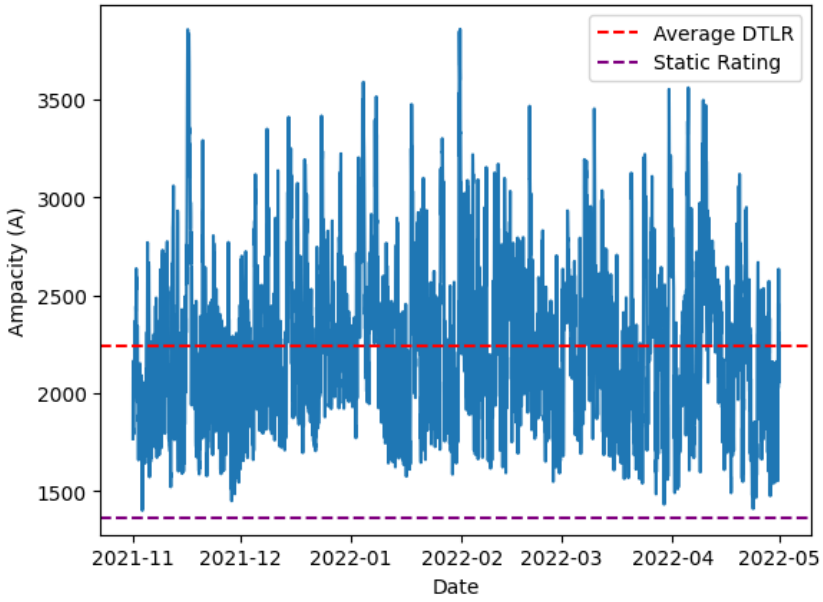

Figure 7. DTLR variation of a single conductor for the six winter months (1 November 2021 to 31 April 2022).

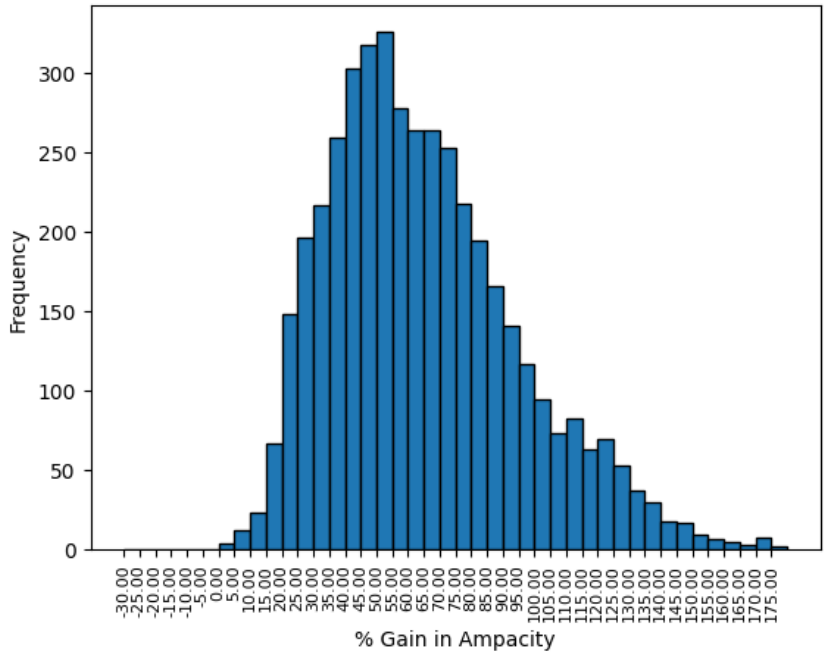

Figure 8. Distribution of percentage gain at a given point of the line during the winter months.

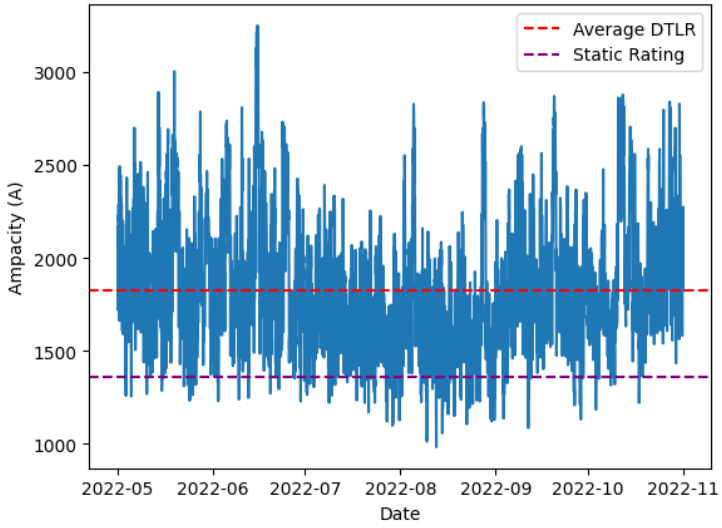

Figure 9. DTLR variation of a single conductor for the six summer months (1 May 2022 to 31 October 2022).

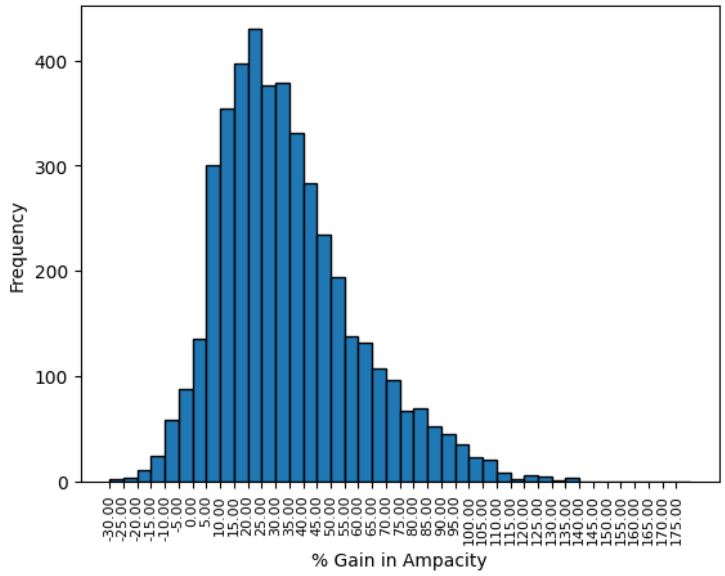

Figure 10. Distribution of percentage gain at a given point of the line during the summer months.

Analyzing the outcome, dynamic behavior of the line ampacity is observed in both winter and summer months due to the fluctuations in weather conditions. According to Figure 7, during the six winter months, the average DTLR for a single conductor across the entire transmission is calculated as 2242.34 A, as indicated by the red dotted line. Therefore, the average gain in the thermal rating for a single conductor across the entire transmission line stands at 883.34 A during the winter months. In terms of power, for the four bundled conductors connected to the 500 kV system, the potential additional power that could be transferred amounts to 1766.68 MW, which gives up to a 64% increase from the nominal rating on average. Figure 8 depicts the distribution of the percentage gain in ampacity in the winter months. This distribution can be identified as a uni-modal right-skewed distribution, as the calculated mean of 65% is greater than the observed majority of the percentage gains, which lie in the range of 45% to 55%. In addition, the maximum percentage gain in the distribution stands at 183.88%, while the minimum percentage amounts to 3%. It is important to note that all the calculated percentage gain values are positive, indicating a consistent opportunity for enhanced power integration to the selected grid during winter months. Furthermore, the above statistical analysis attests to the importance of dynamic line rating calculations, as it reveals the untapped potential for an increased current capacity.

It also indicates that, in real-time scenarios, the lines are often underutilized, leaving room for enhanced power transfer.

During the summer months, the average DTLR for a single conductor across the entire transmission is 1826.83 A, as shown in Figure 9, resulting in an average gain of 467.83 A. The potential additional power that could be transferable through the transmission line is 935.64 MW, which is up to a 34% increase in the nominal rating on average. Conversely, an average loss of 375.78 A in capacity in the summer months is observed. In terms of frequency, the conductor DTLR goes 190 times below the static rating on an hourly basis for the considered six winter months. That is, 4% of the time during the six winter months, the conductor experiences a lower rating than it is rated. This highlights the possibility of overloading the line under the least favorable conditions with the conservative estimates provided by static line ratings. Figure 10 shows the distribution of the percentage gain in the summer months. Similar to the case in winter months, the percentage gain in summer also follows a uni-modal right-skewed distribution. However, the skewness is much more visible in Figure 10, as a major portion of the distribution accounts for lower percentage gain values. Figure 11 allows for a much clearer comparison between the two distributions. Notably, the calculated mean of 34.42% is 30.58% lower when compared with the mean of 65% in the winter months. Accordingly, the majority of the range of values recorded for percentage gains in ampacity in the summer period show only a percentage gain between 15% and 25%, which is much lower than the range observed for the winter months. Furthermore, the minimum gain of negative 27.65% and a relatively low maximum of 139.13% in percentage gain values emphasize the unfavorable conditions during summer months. This can be attributed to the elevated temperatures in the summer period, which are drastically different when compared to the temperatures in the winter periods in the selected region.

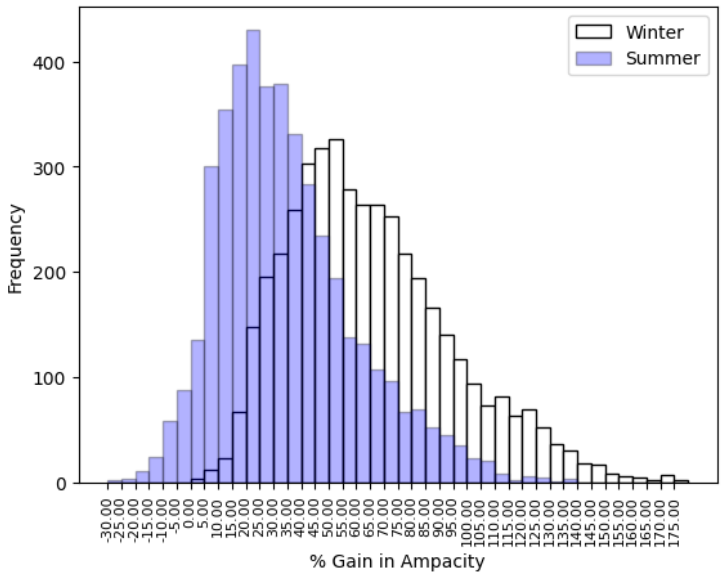

Figure 11. Comparison of percentage gain in ampacity during winter and summer.

To more accurately calculate the variations in the DTLR during a 24 h window, the calculated DTLR values as indicated in Figures 7 and 9 were taken into account and the average DTLR for each hour was assessed for the six months in winter and summer separately. The scatter plots in Figures 12 and 13 show the calculated average DTLR for each hour during the winter and summer, respectively. These plots provide a clear picture of how the EATL transmission capacity changes throughout a day in winter and summer. The peaks in the plots illustrate the time of the day when the transmission line can effectively transmit higher currents due to favorable weather conditions, and troughs indicate when the line experiences adverse weather conditions during the day.

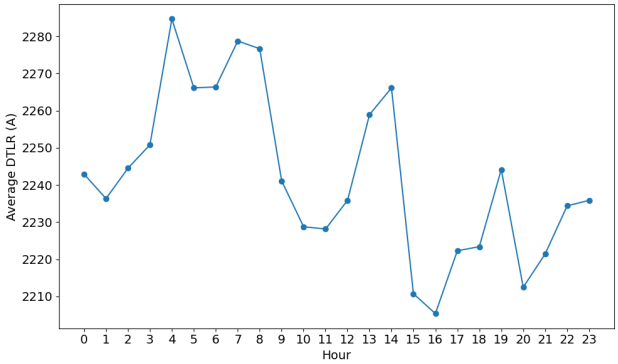

Figure 12. Hourly average DTLR variation throughout a day in winter.

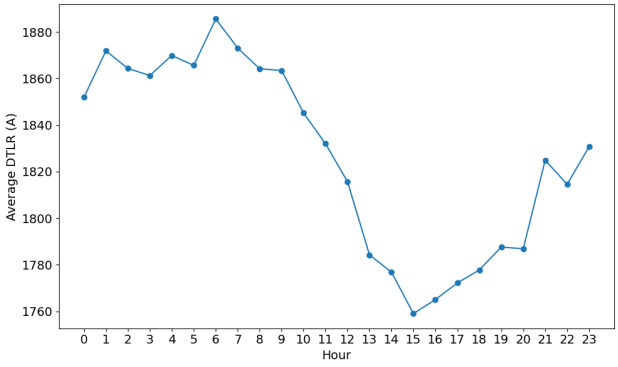

Figure 13. Hourly average DTLR variation throughout a day in summer.

5.2. Wind Power Generation

The performance of a single turbine at JWPP2 was assessed for both the winter and summer according to its turbine power curve and weather data. Figure 14 illustrates the potential power output from a single turbine during January. According to the calculations, it is evident that a single turbine can generate an average of 2.85 MW of power. Figure 15 highlights the variation in the average power output of a turbine throughout the day, with peak generation occurring between 13:00 and 15:00 during the winter months. This suggests that the turbine's performance varies over the day. Furthermore, the total power plant consisting of 13 turbines could supply 37.11 MW to the EATL transmission corridor on average.

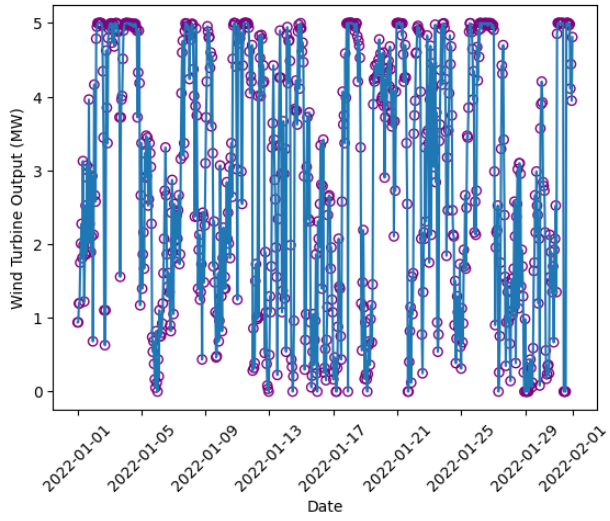

Figure 14. Power generated by a single turbine in JWPP2 in January.

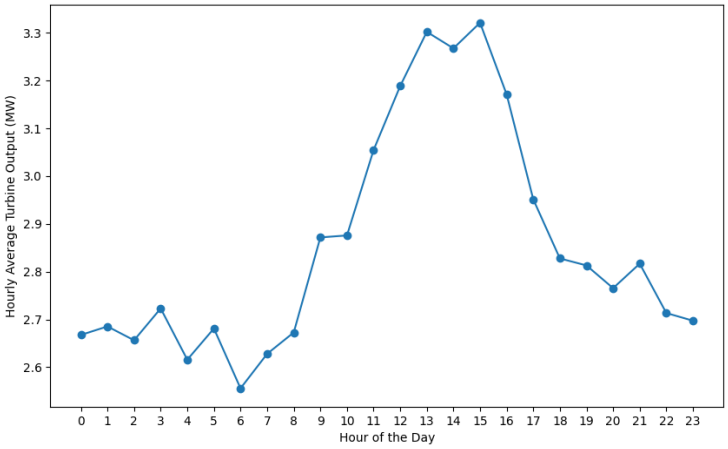

Figure 15. Average turbine output variation in JWPP2 for a day.

5.3. GHG Reduction

As illustrated by the key pollutants from coal-fired power plants listed in Table 2, the emission reductions were calculated for the scenario detailed in Section 5.2. Therefore, considering the situation where the transmission line is fully utilized and the additional demand is supplied from the wind energy generated from the two wind plants using DTLR, the average reduction in GHG emissions was calculated as presented in Table 5. These figures highlight the potential pollution reductions when coal-fired power plants are replaced with renewable energy sources, utilizing DTLR.

Table 5. GHG emission reductions at the JWPP2 wind plant by using DTLR.

Compound	**Avg. (t/h) from JWPP2**
Carbon Dioxide	13.78
Sulphur Dioxide	0.10
Nitrogen Oxides	0.067
Methane	15.79
Mercury	1.51×10^{-8}

6. Discussion

Integration of DTLR into HVDC transmission systems is of significant importance for several reasons. As illustrated in Figures 7 and 9, the significant fluctuations in the DTLR reveal the dynamic interaction with time. In general, the winter months exhibit a greater increase in current carrying capacity above the SR. In contrast, there are some instances during the summer when the DTLR is lower than the SR. This is due to the elevated ambient temperatures in summer, which lead to higher line temperatures, causing a reduced line capacity. In contrast, during winter, lower ambient temperatures allow for more heat dissipation from the line, allowing for higher dynamic ratings. The influence of wind is crucial in DTLR by allowing more convective cooling during high wind conditions, potentially improving the capacity of the line. This might explain the variations in line ratings over the day or year.

According to the results described in Section 5.1, on average, the line rating can increase from its nominal value by up to 64% during winter and 34% during summer. Consequently, the total line gains an additional capacity of 1766.68 MW during winter and 935.66 MW during summer. However, since the focus of this study is on an HVDC transmission line, it would not be possible to use all of the capacity provided by DTLR in all cases. The maximum additional capacity that can be used would be limited by the overloading capability of the connected equipment, especially the converters. On a positive note, as noted in the examples described in Section 1, the overloading capability of HVDC

systems is already being leveraged commercially. This presents an opportunity for HVDC transmission operators to use the advantages of DTLR to meet increasing demand and contribute to reducing GHG emissions.

Assuming a conservative 5% overload for converters for a brief period and considering the examples in Section 1, this still gives a 100 MW additional capacity which can be used during peak demand hours during the day. As demonstrated by the case study in Section 5.1, the excess capacity provided by DTLR is more than enough to compensate for the 100 MW allowed. However, more studies are needed to investigate the overloading capacity of the HVDC converters. Such explorations will enable the strategic utilization of the total excess transmission capacity provided by DTLR.

According to wind power generation calculations, on average, JWPP2 independently contributes 37.11 MW to the line (with the current configuration of 13 turbines). Additionally, the fluctuations in DTLR over 24 hours, as illustrated in Figure 12, are correlated with the changing ambient conditions throughout the day. This provides valuable insights when the DTLR is higher and when it is lower. By aligning these fluctuations with wind power generation patterns (cf. Figure 15), more renewable energy can be optimally dispatched to the grid without any curtailment. This strategic approach, based on DTLR indications of a higher capacity, enables more efficient integration of renewable energy.

Furthermore, from the turbine power output graph in Figure 14, it is evident that the average power generated by a single turbine is less than its rated capacity. The average output slightly surpasses 50% of its nominal rating. This underutilization allows developers to construct much larger wind plants and utilities to connect them to the existing network. Furthermore, in this case study, it has been found that it would take 35 Enercon E-147 turbines to generate a power equal to the excess 100 MW achieved by DTLR. This represents a significant contribution to the reduction in greenhouse gas emissions and underscores the potential to scale up wind power projects to maximize their environmental impact.

7. Conclusions

As the electrical industry is facing challenges in moving forward with net-zero emission goals, efficiently incorporating more renewable energy into the grid becomes crucial. The surge in demand and the addition of more renewable energy to the system raise doubts about the sufficiency of the existing infrastructure and highlight the need for additional investments in new assets. According to the literature, maximizing the utilization of conductors has been predominantly studied in AC systems with the concept of DTLR. By identifying the opportunity to apply DTLR in HVDC systems for seamless renewable integration, this study aims to bridge this knowledge gap.

Essentially, the results show that incorporating DTLR into an HVDC line allows for more capacity than when using the SR of the conductor. Importantly, the excess capacity offered by DTLR changes with time, mirroring the changes in ambient conditions. These temporal fluctuations highlight the importance of selecting the right moment to employ dynamic capacity, allowing utilities to capture their full benefits. Allocating additional capacity for a few hours enables tapping more renewable energy into the grid. By doing so, pollutant-emitting coal-fired power plants can be replaced by renewable sources, thereby reducing GHG emissions.

Nevertheless, the realization of the full capacity offered by DTLR in HVDC systems is restricted due to the limitations of the overloading capability of the converters. This limitation unveils many opportunities to conduct more research on the overloading of HVDC converters to fully utilize the maximum possible benefits of DTLR. By factoring in the contribution from DTLR, developers and utilities can move forward with net-zero emission goals with significantly less investment in the transmission infrastructure while adding more renewable generation to the grid.

In conclusion, in this study, we have demonstrated a pioneering application of DTLR which is specifically tailored for HVDC transmission corridors. This study would be one of the first studies to apply the concept of DTLR to an HVDC transmission corridor utilizing

a real-time case study and real-time meteorological data. Our findings highlight the importance of future research in this area to assess the converter capabilities and optimize the deployment of real-time weather data to enhance the efficiency, reliability, and sustainability of HVDC grids. It is also shown how the same technique used in traditional AC systems can be used for HVDC systems, but it significantly varies, necessitating consideration of additional equipment such as converters and associated control strategies. Additionally, the same concepts and benefits from utilizing DTLR in HVDC corridors are not only limited to renewable generation but can also be extended to other types of power generation, i.e., essentially any type of power injection.

Author Contributions: Conceptualization, P.M., G.K. and V.P.; methodology, P.M. and G.K.; software, V.P.; validation, P.M., G.K. and V.P.; formal analysis, P.M., G.K. and V.P.; investigation, V.P.; resources, P.M.; data curation, V.P.; writing—original draft preparation, V.P.; writing—review and editing, P.M. and G.K.; visualization, V.P.; supervision, P.M. and G.K.; project administration, P.M.; funding acquisition, P.M. All authors have read and agreed to the published version of the manuscript.

Funding: This research was funded by the Natural Sciences and Engineering Research Council (NSERC) of Canada, grant number ALLRP 549804-19, and by the Alberta Electric System Operator, AltaLink, ATCO Electric, ENMAX, EPCOR Inc., and FortisAlberta.

Data Availability Statement: The original contributions presented in the study are included in the article, further inquiries can be directed to the corresponding author.

Conflicts of Interest: The authors declare no conflicts of interest.

Abbreviations

The following abbreviations are used in this manuscript:

AC	alternating current
ACIS	Alberta Climate Information Service
ACSR	aluminium conductor steel-reinforced
AESO	Alberta Electric System Operator
DTLR	dynamic thermal line rating
EATL	Eastern Alberta transmission line
GHG	greenhouse gas
JWPP	Jenner wind power project
HVDC	high-voltage direct current
LCC	line-commutated converter
SR	static rating
VSC	voltage source converter
WATL	Western Alberta transmission line

References

1. Kacejko, P.; Wydra, M.; Nowak, W.; Szpyra, W.; Tarko, R. Advantages, Benefits, and Effectiveness Resulting from the Application of the Dynamic Management of Transmission Line Capacities. In Proceedings of the 2018 15th International Conference on the European Energy Market (EEM), Lodz, Poland, 27–29 June 2018; pp. 1–5. [CrossRef]
2. Bao, W.; Yan, Y.; Zhang, W.; Xin, J.; Li, Z.; Tang, R. Field study of a novel dynamic rating system for power transmission lines. In Proceedings of the 2015 5th International Conference on Electric Utility Deregulation and Restructuring and Power Technologies (DRPT), Changsha, China, 26–29 November 2015; pp. 1726–1731. [CrossRef]
3. Foss, S.D.; Lin, S.H.; Fernandes, R.A. Dynamic Thermal Line Ratings Part I Dynamic Ampacity Rating Algorithm. *IEEE Trans. Power Appar. Syst.* **1983**, *PAS-102*, 1858–1864. [CrossRef]
4. Bhattarai, B.P.; Gentle, J.P.; McJunkin, T.; Hill, P.J.; Myers, K.S.; Abboud, A.W.; Renwick, R.; Hengst, D. Improvement of Transmission Line Ampacity Utilization by Weather-Based Dynamic Line Rating. *IEEE Trans. Power Deliv.* **2018**, *33*, 1853–1863. [CrossRef]
5. Fernandez, E.; Albizu, I.; Bedialauneta, M.; Mazon, A.; Leite, P. Review of dynamic line rating systems for wind power integration. *Renew. Sustain. Energy Rev.* **2016**, *53*, 80–92. [CrossRef]
6. Michiorri, A.; Nguyen, H.M.; Alessandrini, S.; Bremnes, J.B.; Dierer, S.; Ferrero, E.; Nygaard, B.E.; Pinson, P.; Thomaidis, N.; Uski, S. Forecasting for dynamic line rating. *Renew. Sustain. Energy Rev.* **2015**, *52*, 1713–1730. [CrossRef]
7. Morgan, V. Rating of bare overhead conductors for continuous currents. *Proc. Inst. Electr. Eng.* **1967**, *114*, 1473–1482. [CrossRef]

8. House, H.E.; Tuttle, P.D. Current-Carrying Capacity of ACSR. *Trans. Am. Inst. Electr. Eng. Part III Power Appar. Syst.* **1958**, *77*, 1169–1173. [CrossRef]
9. Davis, M. A new thermal rating approach: The real time thermal rating system for strategic overhead conductor transmission lines – Part I: General description and justification of the real time thermal rating system. *IEEE Trans. Power Appar. Syst.* **1977**, *96*, 803–809. [CrossRef]
10. Raniga, J.; Rayudu, R. Dynamic rating of transmission lines-a New Zealand experience. In Proceedings of the 2000 IEEE Power Engineering Society Winter Meeting. Conference Proceedings (Cat. No.00CH37077), Singapore, 23–27 January 2000; Volume 4, pp. 2403–2409. [CrossRef]
11. Yip, T.; An, C.; Lloyd, G.; Aten, M.; Ferri, B. Dynamic line rating protection for wind farm connections. In Proceedings of the 2009 CIGRE/IEEE PES Joint Symposium Integration of Wide-Scale Renewable Resources Into the Power Delivery System, Glasgow, UK, 17–20 March 2008; pp. 1–5.
12. Cloet, E.; Lilien, J.L. Uprating Transmission Lines through the use of an innovative real-time monitoring system. In Proceedings of the 2011 IEEE PES 12th International Conference on Transmission and Distribution Construction, Operation and Live-Line Maintenance (ESMO), Providence, RI, USA, 16–19 May 2011; pp. 1–6. [CrossRef]
13. Kim, S.D.; Morcos, M.M. An Application of Dynamic Thermal Line Rating Control System to Up-Rate the Ampacity of Overhead Transmission Lines. *IEEE Trans. Power Deliv.* **2013**, *28*, 1231–1232. [CrossRef]
14. Glaum, P.; Hofmann, F. Leveraging the existing German transmission grid with dynamic line rating. *Appl. Energy* **2023**, *343*, 121199. [CrossRef]
15. Wijethunga, A.; Wijayakulasooriya, J.; Ekanayake, J.; De Silva, N. Conductor temperature based low cost solution for dynamic line rating calculation of power distribution lines. In Proceedings of the 2015 IEEE 10th International Conference on Industrial and Information Systems (ICIIS), Peradeniya, Sri Lanka, 18–20 December 2015; pp. 128–133. [CrossRef]
16. Negari, S.; Raahemifar, K.; Xu, D. Predictive line rating in underground transmission lines going beyond dynamic line rating. In Proceedings of the 2016 IEEE Canadian Conference on Electrical and Computer Engineering (CCECE), Vancouver, BC, Canada, 15–18 May 2016; pp. 1–6. [CrossRef]
17. Hertem, D.V.; Gomis-Bellmunt, O.; Liang, J. LCC-HVDC Systems. In *HVDC Grids—For Offshore and Supergrid of the Future*; John Wiley & Sons: Hoboken, NJ, USA, 2016; Chapter 3.2.
18. Pytlak, P.; Musilek, P.; Doucet, J. Using Dynamic Thermal Rating systems to reduce power generation emissions. In Proceedings of the 2011 IEEE Power and Energy Society General Meeting, Detroit, MI, USA, 24–28 July 2011; pp. 1–7. [CrossRef]
19. Alberta Electric System Operator. AESO 2022 Long-term Transmission Plan. In *Technical Report*; Alberta Electric System Operator: Calgary, AB, Canada, 2022.
20. Rajaram, H.R.; Balamurugan, G. A Study on Green House Gas Mitigation from Solar Parks in India. In Proceedings of the 2020 International Conference and Utility Exhibition on Energy, Environment and Climate Change (ICUE), Pattaya, Thailand, 20–22 October 2020; pp. 1–8. [CrossRef]
21. Paraschiv, L.S.; Paraschiv, S. Contribution of renewable energy (hydro, wind, solar and biomass) to decarbonization and transformation of the electricity generation sector for sustainable development. *Energy Rep.* **2023**, *9*, 535–544. [CrossRef]
22. Fernandez, E.; Albizu, I.; Buigues, G.; Valverde, V.; Etxegarai, A.; Olazarri, J.G. Dynamic line rating forecasting based on numerical weather prediction. In Proceedings of the 2015 IEEE Eindhoven PowerTech, Eindhoven, The Netherlands, 29 June–2 July 2015; pp. 1–6. [CrossRef]
23. Abdelkader, S.; Morrow, D.; Fu, J.; Abbot, S. Field Measurement Based PLS Model for Dynamic Rating of Overhead Lines in Wind Intensive Areas. *Renew. Energy Power Qual. J.* **2013**, *1*, 808–813. [CrossRef]
24. Schell, P.; Lambin, J.; Godard, B.; Nguyen, H.M.; Lilien, J.L. Using Dynamic Line Rating to Minimize Curtailment of Wind Power Connected to Rural Power Networks. In Proceedings of the 10th International Workshop on Large-Scale Integration of Wind Power into Power Systems, Aarhus, Denmark, 25–26 October 2011.
25. Talpur, S.; Wallnerstrom, C.J.; Flood, C.; Hilber, P. Implementation of Dynamic Line Rating in a Sub-Transmission System for Wind Power Integration. *Smart Grid Renew. Energy* **2015**, *6*, 233–249. [CrossRef]
26. Sun, J.; Li, M.; Zhang, Z.; Xu, T.; He, J.; Wang, H.; Li, G.J. Renewable energy transmission by HVDC across the continent: system challenges and opportunities. *CSEE J. Power Energy Syst.* **2017**, *3*, 353–364. [CrossRef]
27. Borbáth, T.; Chaffey, G.; Kaushal, A.; Van Hertem, D. Dynamic rating of HVDC interconnectors. In Proceedings of the 19th International Conference on AC and DC Power Transmission (ACDC 2023), Glasgow, UK, 1 March 2023; Volume 2023, pp. 254–259. [CrossRef]
28. Britned. Dynamic Rating Trial. Available online: https://www.britned.com/knowledge-base/britned-basics/dynamic-rating-trial/ (accessed on 25 September 2023).
29. Nemo Link. Nemo Link Announces Transient Overflow Facility. Available online: https://www.nemolink.co.uk/news-news/nemo-link-announces-transient-overflow-facility-2/ (accessed 25 September 2023).
30. Nord Pool Group. Principles for Determining the Transfer Capacities. Available online: https://www.nordpoolgroup.com/493abd/globalassets/download-center/tso/principles-for-determining-the-transfer-capacities-2023-03-23.pdf (accessed 25 September 2023).

31. Aidong, X.; Xiaochen, W.; Chao, H.; Xiaoming, J.; Peng, L. Study on Overload Capability and Its Application of HVDC Transmission System in China Southern Power Grid. In Proceedings of the 2007 IEEE Power Engineering Society Conference and Exposition in Africa—PowerAfrica, Johannesburg, South Africa, 16–20 July 2007; pp. 1–4. [CrossRef]
32. Alberta Electric System Operator. *AESO 2020 Long-Term Transmission Plan*; Technical Report; Alberta Electric System Operator: Calgary, AB, Canada, 2020.
33. Alberta Electric System Operator. *Current Supply Demand Report*;Technical Report; Alberta Electric System Operator: Calgary, AB, Canada, 2023.
34. CIGRE WG B2.42. Guide for Thermal Rating Calculations of Overhead Lines. In *Technical Report Technical Brochure 601*; CIGRE: Paris, France, 2014.
35. *IEEE Std 738-2012 (Revision of IEEE Std 738-2006–Incorporates IEEE Std 738-2012 Cor 1-2013)*; IEEE Standard for Calculating the Current-Temperature Relationship of Bare Overhead Conductors. IEEE: Piscataway, NJ, USA, 2013; pp. 1–72. [CrossRef]
36. Staszewski, L.; Rebizant, W. The differences between IEEE and CIGRE heat balance concepts for line ampacity considerations. In Proceedings of the 2010 Modern Electric Power Systems, Wroclaw, Poland, 20–22 September 2010; pp. 1–4.
37. Morgan, V. The thermal rating of overhead-line conductors Part I. The steady-state thermal model. *Electr. Power Syst. Res.* **1982**, *5*, 119–139. [CrossRef]
38. Schmidt, N. Comparison between IEEE and CIGRE ampacity standards. *IEEE Trans. Power Deliv.* **1999**, *14*, 1555–1559. [CrossRef]
39. Erdinç, F.G.; Erdinç, O.; Yumurtacı, R.; Catalão, J.P.S. A Comprehensive Overview of Dynamic Line Rating Combined with Other Flexibility Options from an Operational Point of View. *Energies* **2020**, *13*, 6563. [CrossRef]
40. Fernandez, E.; Albizu, I.; Bedialauneta, M.; Mazon, A.; Leite, P. Dynamic line rating systems for wind power integration. In Proceedings of the IEEE Power and Energy Society Conference and Exposition in Africa: Intelligent Grid Integration of Renewable Energy Resources (PowerAfrica), Johannesburg, South Africa, 9–13 July 2012; pp. 1–7. [CrossRef]
41. Foss, S.D.; Lin, S.H.; Stillwell, H.R.; Fernandes, R.A. Dynamic Thermal Line Ratings Part II Conductor Temperature Sensor and Laboratory Field test Evaluation. *IEEE Trans. Power Appar. Syst.* **1983**, *PAS-102*, 1865–1876. [CrossRef]
42. Engelhardt, J.; Basu, S. Design, installation, and field experience with an overhead transmission dynamic line rating system. In Proceedings of 1996 Transmission and Distribution Conference and Exposition, Los Angeles, CA, USA, 15–20 September 1996; pp. 366–370.. [CrossRef]
43. Akpolat, A.N.; Nese, S.V.; Dursun, E. Towards to smart grid: Dynamic line rating. In Proceedings of the 2018 6th International Istanbul Smart Grids and Cities Congress and Fair (ICSG), Istanbul, Turkey, 25–26 April 2018; pp. 96–100. [CrossRef]
44. Black, C.R.; Chisholm, W.A. Key Considerations for the Selection of Dynamic Thermal Line Rating Systems. *IEEE Trans. Power Deliv.* **2015**, *30*, 2154–2162. [CrossRef]
45. Ahmed, I.; Rehan, M.; Basit, A.; Hong, K.S. Greenhouse gases emission reduction for electric power generation sector by efficient dispatching of thermal plants integrated with renewable systems. *Sci. Rep.* **2022**, *12*, 12380. [CrossRef] [PubMed]
46. Alberta Public Affairs Bureaur. Jenner Wind Project (Phase 1, 2, and 3). Available online: https://majorprojects.alberta.ca/details/Jenner-Wind-Project-Phase-1-2-and-3/4443 (accessed on 4 October 2023).
47. For International Development Cooperation RoAid, R.A. The Expansion of the Qartli Wind Farm—A Study of Opportunity, 2019. Technical Report; Ridgeline Industrial, Bucuresti, Romania, 2020. Available online: https://ridgeline-industrial.ro/Georgia_III_Report-50MW_and_Hydrogen_V1_10-Nov-2020.pdf (accessed on 20 August 2023).
48. Alberta Climate Information Service. Available online: https://acis.alberta.ca (accessed on 20 August 2023).

Disclaimer/Publisher's Note: The statements, opinions and data contained in all publications are solely those of the individual author(s) and contributor(s) and not of MDPI and/or the editor(s). MDPI and/or the editor(s) disclaim responsibility for any injury to people or property resulting from any ideas, methods, instructions or products referred to in the content.